Overlap-Save FBMC receivers for massive MIMO systems

Fatima Hamdar, Jeremy Nadal, Charbel Abdel Nour, Amer Baghdadi

Overlap-Save FBMC receivers for massive MIMO systems

Fatima Hamdar, Jeremy Nadal, Charbel Abdel Nour, and Amer Baghdadi

***Abstract*—Massive multiple-input multiple-output (mMIMO) systems and filtered multi-carrier waveforms have recently emerged as hot research topics in next-generation wireless networks. This paper extends the use of Overlap-Save Filter Bank Multi-Carrier (FBMC) receivers to mMIMO communication systems and investigates the corresponding FBMC transceiver advantages over OFDM. To this aim, we derived the signal-to-interference ratio (SIR) expressions analytically under several channel impairments such as timing offsets and carrier frequency offsets. Furthermore, we conducted an asymptotic study on the performance of FBMC augmented with our proposed receivers in the context of massive MIMO systems. While still outperforming OFDM, results for FBMC show that increasing the number of base station (BS) antennas does not increase the SINR unboundedly. We have validated the proposed analytical study by comparing its results with those obtained from Monte Carlo simulations and confirmed the superiority of the proposed receivers over those in mMIMO literature. Moreover, analytical and simulation results confirm that the Overlap-Save FBMC receiver can support asynchronous communications in the context of mMIMO, a cornerstone for grant-free communications and massive access.**

***Index Terms*—Beyond 5G, massive MIMO, analytical performance, FBMC/OQAM, Overlap-Save based FBMC receivers, OFDM, asynchronous communication, relaxed synchronization, QuaDRiGa channel**

I. Introduction

Addressing part of the requirements of the upcoming 6G wireless communication network, Massive multiple-input multiple-output (mMIMO) emerges as a pivotal solution. Indeed, it enhances the spectral efficiency, throughput, and quality of service. In mMIMO systems, the base station (BS) is equipped with a large number of antennas adeptly catering to multiple users and mitigating small-scale fading effects [2]. Furthermore, mMIMO mitigates fast fading and multi-user (MU) interference while implementing simple linear signal processing techniques [3].

Adopted in multiple standards including fifth generation (5G) systems [4], the multi-carrier modulation orthogonal frequency division multiplexing (OFDM) enables efficient mMIMO integration [5]. However, the yearly growth in user density [6] has shown OFDM limitations, especially in an uplink multi-user scenario. Therefore, maximizing spectrum efficiency by enabling multiple users to coexist within the same OFDM symbol (intra-band communication) becomes imperative. Nonetheless, this objective contradicts OFDM principles since the orthogonality property, which guarantees interference-free multi-user access, is upheld only when stringent time and frequency synchronization constraints are met [7]–[9]. Indeed, the presence of any carrier frequency offsets (CFO) in the received uplink signal results in substantial inter-carrier-interference (ICI) due to the inherently high out-of-band-power-leakage (OOBPL) of OFDM. This can arise when low-cost devices cannot afford precise local oscillators. Moreover, it is essential to ensure that the time delay difference between received OFDM signals does not exceed the duration of the cyclic prefix (CP). Otherwise, timing advance mechanism [10] must be employed to adjust signal delays, which is unsuitable for low-latency applications and machine-type communications, where low-cost devices sporadically transmit data.

As an alternative to the timing advance mechanism, two simplified time synchronization procedures can be considered. The first is the relaxed synchronization scenario, where multiple users transmit data within a common time reference. However, because each user is located at a different distance from the BS, their signals experience a different propagation delay, leading to a specific timing offset (TO) that the receiver must be able to compensate for in order to maintain energy efficiency. The second scenario is the asynchronous communication scenario, where users transmit data without considering any time reference, resulting in a time mismatch between users that can be as large as 50% of the symbol duration. However, the potential gains of MU-mMIMO-OFDM systems heavily rely on accurate frequency and time synchronization across multiple users, which is challenging owing to the presence of several CFOs/ TOs at the BS [11]. Accurately estimating and compensating MU CFO/TO differs significantly from conventional single-user (SU) systems [12]–[15]. Hence, retaining subcarrier orthogonality typically requires computationally expensive mMIMO techniques [16]. Considering these OFDM shortcomings, the promising benefits of MU-mMIMO systems, and the stringent requirements of beyond 5G systems, there is renewed interest in alternative waveforms to address OFDM drawbacks and fully leverage mMIMO technologies.

Filter bank multicarrier with offset quadrature amplitude modulation (FBMC/OQAM) is one of the promising alternative waveform to OFDM that has been investigated in the context of 5G. Recently, innovative contributions have been proposed for FBMC/OQAM in single-input-single-output (SISO) systems [17], [18]. With the same duration as one OFDM symbol, the *short* Near Perfect Reconstruction-1 (NPR1) prototype filter (PF) was proposed in [17]. Its usage results in a significant reduction in latency, hardware complexity, and energy consumption. When combined with short PFs such as

IMT Atlantique, Lab-STICC, UMR CNRS 6285, F-29238 Brest, France, CORRESPONDING AUTHOR: F. HAMDAR (e-mail: fatima.hamdar@imt-atlantique.fr).

This work largely extends the results in [1].

the NPR1 the OS-FBMC receiver proposed in [18] enhances the robustness against doubly dispersive channels and supports asynchronous communications.

To overcome the aforementioned drawbacks of OFDM in MU-mMIMO systems, we extend the latest FBMC/OQAM advantages through the proposal of OS-based MU-mMIMO receivers. Furthermore, we derive signal-to-interference-plus-noise ratio (SINR) analytical expressions for the proposed receivers over different channel impairments including the presence of TOs and CFOs. These have been used to evaluate the performance of the proposed FBMC/OQAM MU-mMIMO transceivers under different system scenarios over realistic channel models and without the need for time-consuming Monte Carlo simulations. The specific contributions presented in this paper can be summarized as follows:

1) Proposal of overlap-save (OS)-based FBMC receivers for MU-mMIMO systems.
2) Derivation of the corresponding analytical signal-to-interference ratio (SIR) expressions in the presence of CFOs and TOs.
3) Derivation of an asymptotic analytical expression of the SINR saturation level for the proposed OS-FBMC receivers.
4) Evaluation and validation of their performance under the 3D-urban-macro non-line-of-sight (Uma-NLOS) and 3GPP-38.901-rural macro (Rma) channel models with several channel impairments.

The rest of the paper is organized as follows. In Section II, we go through relevant existing FBMC and OFDM transceivers in the context of mMIMO to pave the way for the derivations provided in this work. The proposed OS-based FBMC receivers for MU-mMIMO are detailed in Section III. In Section IV, we provide the analytical derivation of the SIR in the presence of CFOs and TOs, followed by an asymptotic evaluation of the SINR level for the proposed receivers. Section V describes the channel model along with the antenna array structure and the considered simulation parameters. Sections VI to IX provide the validation results of the analytical derivation, evaluate the efficiency of the proposed OS-based FBMC receivers, and compare the results of the proposal to the conventional OFDM receiver in different transmission scenarios. Section X provides complexity assessment of the proposed receivers. Finally, section XI concludes the paper.

II. Relevant multi-carrier transceivers in the context of massive MIMO

A. The OFDM transceiver

The OFDM transmitter is implemented using an inverse fast fourier transform (IFFT) of size M, where M is the total number of subcarriers that may be transmitted [19].

The transmitted signal composed of M samples is obtained at the IFFT output, where a CP of length L_{CP} is added before the first samples. The OFDM receiver performs dual operations with respect to the transmitter for demodulation. Due to the increased dimension of mMIMO systems, a low-complexity detection algorithm is required, such as zero forcing (ZF). The latter entails an equalization matrix defined by $\boldsymbol{C_n}(m) = \boldsymbol{H_n^+}(m)$ for the received symbol n at frequency bin m, where $\boldsymbol{H_n^+}$ is the pseudo inverse operator of the channel frequency response (CFR) matrix. This ZF equalizer performs near-optimally if the number of antennas at the BS tends to infinity [20].

B. The FBMC transceiver

The FBMC modulation may be implemented in two ways: *polyphase* network (PPN)-based [21] and *Frequency Spread* (FS)-based [22]. Similarly to OFDM, the first implementation is composed of one size-M IFFT, followed by one PPN for the filtering stage. The length of the PF, parameterized by the overlapping factor K, determines the PPN processing. Using a short PF (i.e. $K = 1$) significantly reduces the computational complexity and latency. To preserve orthogonality in the real field, the OQAM scheme is used. Therefore, if $\boldsymbol{a_n}(m) \in \mathbb{C}^{U\times 1}$ are the pulse-amplitude modulated (PAM) symbols for the users at time slot n, subcarrier index m, then the baseband signal $\boldsymbol{s}(k)$ is expressed as

$$\boldsymbol{s}(k) = \sum_{n=-\infty}^{+\infty} g\left(k - n\frac{M}{2}\right)\boldsymbol{x_n}(k), \tag{1}$$

with

$$\boldsymbol{x_n}(k) = \sum_{m=0}^{M-1} (-1)^{nm}\boldsymbol{a_n}(m)\phi_n(m)e^{i2\pi\frac{km}{M}}, \tag{2}$$

where g denotes the impulse response of the PF and $\phi_n(m) = i^{n+m}$.

The use of FBMC in mMIMO systems was investigated in [23], with results obtained for a sample set of channel responses generated using the IEEE802.16 broadband channel model (SUI-4) [24]. Simulations confirmed its self-equalization property, which results in a channel flattening effect.

In [25], the authors proposed a simple FBMC PF design aimed at eliminating antenna array correlation, allowing the system to achieve arbitrarily high SINR values as the number of antennas increases. However, OFDM outperforms their proposal, achieving approximately 1.5 dB higher SINR when considering a simple exponentially decaying channel. This performance gap is likely to get even wider when more realistic channel models are considered. In [26], a PPN-FBMC low complexity data detector was implemented, preceded by a mMIMO equalization. However, it was shown that the FBMC waveform is outperformed by OFDM in the context of large-scale MIMO systems over the WINNER-Phase2 channel model due to the PPN structure of the receiver [26]. Since the prior art on FBMC-based mMIMO is still in its early stages, these systems require rigorous inspection and investigation before conclusive results can be drawn.

III. Proposed OS-based FBMC receivers in the context of massive MIMO

The OS-FBMC receiver was proposed for SISO transmissions in [18]. Its primary concept is to combine an OS-based time-domain equalizer with FBMC demodulation. This

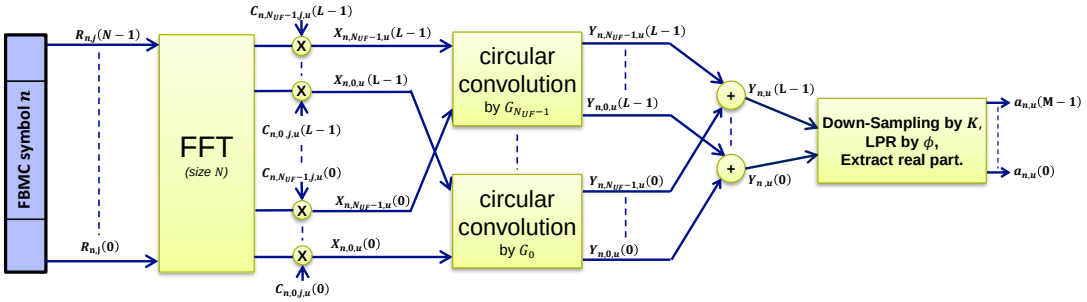

Fig. 1: OS-FBMC/OQAM massive MIMO Receiver.

receiver, combined with the NPR1 short PF, was proven to exhibit enhanced robustness against TOs and long delay spread multipath channels while reducing computational complexity in comparison to existing FBMC receivers presented in the literature [18]. In fact, there is a lot of interest in combining short PF with FBMC since it allows the support of short frame sizes for low latency communications. When compared to long PFs, this can significantly reduce computational complexity and result in improved power efficiency. Thus, implementing the OS-based FBMC receivers in the context of mMIMO becomes particularly appealing. To the best of our knowledge, our work is the first to consider OS-based FBMC receivers with mMIMO.

A. The Overlap-Save FBMC receiver with massive MIMO

Figure 1 depicts the OS-FBMC receiver in the context of mMIMO. Let N_R be the number of antennas deployed at the receiver side, and U be the total number of users. At the output m of the size N FFT, the received signal $R_{n,m}(j)$ at receiver antenna j, symbol index n, is expressed as the size N FFT signal at subcarrier index m:

$$R_{n,m}(j) = \sum_{k=0}^{N-1} r_j \left(k + n\frac{M}{2}\right) e^{-i\frac{2\pi km}{N}}, \tag{3}$$

where r_j is the received signal on the j^{th} antenna in time domain. To ease notations, the received signal of all antennas can be combined into a vector $\boldsymbol{R_n}(m)$ given as

$$\boldsymbol{R_n}(m) = [R_{n,m}(1), ..., R_{n,m}(N_R)]. \tag{4}$$

Note that $\boldsymbol{R_n}(m)$ is a combination of all the signals coming from different users consisting of several FBMC symbols. Similarly to OFDM, MIMO equalization is performed directly after FFT as $\boldsymbol{X_n}(m) = \boldsymbol{C_n}(m) \times \boldsymbol{R_n}(m)$, where $\boldsymbol{X_n}(m)$ is the equalized signal for all users, and $\boldsymbol{C_n}(m) \in \mathbb{C}^{U\times N_R}$ is the zero-forcing equalizer matrix at frequency bin m defined in Section II-A.

Then, N_{UF} stages of circular convolution by the frequency shifted responses of the PF is performed on $\boldsymbol{X_n}(m)$, where N_{UF} is an integer number referred to as the up-sampling factor used for the OS technique. Thus, the output of each filtering stage vector is

$$\boldsymbol{Y_n}(m,\ell) = \sum_{p=-\Delta}^{\Delta} G_\ell(p)\boldsymbol{X_n}\Big(\ell + (m-p)N_{UF}\Big), \tag{5}$$

where $\Delta = (N_G - 1)/2$, N_G denotes the number of non-truncated filter coefficients, and G is the frequency shifted response of the PF that can be deduced from its impulse response g as follows

$$G_\ell(p) = e^{i\frac{\pi\ell}{N_{UF}}} \sum_{k=0}^{M-1} g(k) e^{i\frac{2\pi\ell(k-M/2)}{N}} e^{-i\frac{2\pi pk}{M}}. \tag{6}$$

The analysis filter bank (AFB) output $\boldsymbol{Y_n}(m)$, is obtained by summing each filtering stage vector outputs as follows

$$\boldsymbol{Y_n}(m) = \sum_{\ell=0}^{N_{UF}-1} \boldsymbol{Y_n}(m,\ell), \tag{7}$$

with $m \in [\![0, M-1]\!]$. Finally, the transmitted data symbols $\hat{\boldsymbol{a}}_{\boldsymbol{n}}$(m) of all users are recovered after extracting the real part of the down-sampled (by K; K = 1 for short filters) and linear phase rotated ϕ_n filtering stage outputs

$$\hat{\boldsymbol{a}}_{\boldsymbol{n}}(m) = \Re\Big(\boldsymbol{Y_n}(Km)\phi_n^*(m)\Big). \tag{8}$$

B. Overlap-Save-Block FBMC receiver with massive MIMO

The OSB-FBMC receiver can be seen as an OS-FBMC receiver where the FFT is applied on a block of FBMC symbols. Hence, only one FFT is required to process all symbols in a given block. Furthermore, in the particular scenario of low mobility, it can be sufficiently accurate to assume that the channel response remains static over a given block, which reduces the equalization complexity. This is particularly interesting in mMIMO systems since the equalization step is quite complex. Indeed, through similar demodulation steps to OS-FBMC, at the output m of the size N FFT, the received signal $R_{n,m,b}(j)$ at receiver antenna j, symbol index n in a block b, is expressed as

$$R_{n,m,b}(j) = \sum_{k=0}^{N-1} r_{b,j} \left(k + n\frac{M}{2}\right) e^{-i\frac{2\pi km}{N}}. \tag{9}$$

Similarly, the equalized signal for all users $\boldsymbol{X_{b,n}}(m)$ is

$$\boldsymbol{X_{b,n}}(m) = \boldsymbol{C_{b,n}}(m) \times \boldsymbol{R_{b,n}}(m), \tag{10}$$

where $\boldsymbol{C_{b,n}}(m) \in \mathbb{C}^{U\times N_R}$ is $\boldsymbol{C_n}(m)$ for a block b, and $\boldsymbol{R_{b,n}}(m) = [R_{n,m,b}(1), ..., R_{n,m,b}(N_R)]$ is a combination of all the signals stemming from different users and consisting of several blocks of FBMC symbols.

	Type of impairment			
	CFO		TO	
Steps to be applied	**FBMC-OS**	**FBMC-OSB**	**FBMC-OS**	**FBMC-OSB**
1) Shifted impulse response of the PF ($g_\ell(k)$)	Apply (20) using (6)	Apply (20) using (6)	-	-
2) Effect of transmit & receive PFs ($F_{g,\tilde{g}}$)	Apply (27) using (20)	Apply (27) using (20)	-	Apply (51) using (50)
3) SIR expression	Apply (31) using (27)	Apply (33) using (27)	37.22 dB[1]	Apply (56) using (51)

TABLE I: Step-by-step guide for computing the analytical SIR expressions with CFO or TO.

Hence, if $\hat{\boldsymbol{a}}_{\boldsymbol{n},\boldsymbol{b}}$(m) is the recovered PAM symbol at block $\boldsymbol{b}$ and at FBMC symbol n for all users, we have:

$$\hat{\boldsymbol{a}}_{\boldsymbol{b},\boldsymbol{n}}(m) = \Re\Big(\boldsymbol{Y}_{\boldsymbol{b},\boldsymbol{n}}(Km)\phi_n^*(m)\Big), \tag{11}$$

where $\boldsymbol{Y}_{\boldsymbol{n},\boldsymbol{b}}(m)$ is the AFB output expressed as

$$\boldsymbol{Y}_{\boldsymbol{b},\boldsymbol{n}}(m) = \sum_{\ell=0}^{\mathrm{N}_{UF}-1} \sum_{p=-\Delta}^{\Delta} G_\ell(p)\boldsymbol{X}_{\boldsymbol{b},\boldsymbol{n}}(Km-p,\ell), \tag{12}$$

and N_{UF} is chosen as the lowest possible integer value of $\left\lceil 1+\frac{N_s-1}{2K}\right\rceil$ considering that the FFT size must be superior or equal to the block size N_s.

IV. The proposed analytical study

In this section, we derive analytical SIR expressions in the presence of CFO and TO, as well as an analytical expression for the SINR saturation level in an asymptotic regime (i.e. as the number of antennas N_R at the BS tends to infinity) for each of the proposed receivers in the context of MU-mMIMO. Therefore, the relationship between the transmitted symbols and the recovered symbols must be established in order to get an explicit form of the analytical SIR expressions.

A. Analytical SIR expression in the presence of CFO

a) OS Receiver: The expression of the received signal by the j^{th} BS antenna provided in (3) can be rewritten as

$$R_{n,m,\ell}(j) = \sum_{k=0}^{N-1} r_j\left(k+n\frac{M}{2}\right) e^{-i\frac{2\pi k(N_{UF}m+\ell)}{N}}. \tag{13}$$

Equivalently, the complete $N_R \times 1$ received signal which is a combination of all the signals stemming from different users consisting of several FBMC symbols can be expressed as

$$\begin{aligned}\boldsymbol{R}_{\boldsymbol{n}}(m,\ell) &= \sum_{k=0}^{N-1} \boldsymbol{r}\left(k+n\frac{M}{2}\right) e^{-i\frac{2nk(N_{UF}m+\ell)}{N}} \\ &= \sum_{s=0}^{N_{UF}-1}\sum_{k=0}^{M-1} \boldsymbol{r}(p'_n)\times P,\end{aligned} \tag{14}$$

where $p'_n = k+\frac{M}{2}(2s+n)$ and

$$\boldsymbol{R}_n(m,\ell) = [R_{n,m,\ell}(1),...,R_{n,m,\ell}(N_R)], \tag{15}$$

$$\boldsymbol{r}(k) = [r_1(k),...,r_{N_R}(k)], \tag{16}$$

$$P = e^{-i\frac{2\pi s\ell}{N_{UF}}} e^{-i\frac{2\pi km}{M}} e^{-i\frac{2\pi k\ell}{N_{UF}M}}. \tag{17}$$

After equalization, the frequency domain equalized signal can be expressed as

$$\begin{aligned}\underbrace{\boldsymbol{X}_n(m,l)}_{\in\mathbb{C}^{U\times 1}} &= \underbrace{\boldsymbol{C}_n(m,\ell)}_{\in\mathbb{C}^{U\times N_R}} \times \underbrace{\boldsymbol{R}_n(m,\ell)}_{\in\mathbb{C}^{N_R\times 1}} \\ &= \boldsymbol{C}_n(m,\ell)\times \sum_{s=0}^{N_{UF}-1}\sum_{k=0}^{M-1} \boldsymbol{r}(p'_n)\times P.\end{aligned} \tag{18}$$

This is followed by a filtering stage as previously mentioned in Section III-A, which is rearranged in the time domain. Then the ℓ^{th} AFB output is

$$\underbrace{\boldsymbol{Y}_n(m,\ell)}_{\in\mathbb{C}^{U\times 1}} = \boldsymbol{C}_n(m)\sum_{s=0}^{N_{UF}-1}\sum_{k=0}^{M-1} g_\ell(k)\boldsymbol{r}(p'_n)\frac{P}{e^{-i\frac{2\pi k\ell}{N_{UF}M}}}, \tag{19}$$

where $g_\ell(k)$ represents the ℓ^{th} impulse response of the PF defined as

$$g_\ell(k) = (-1)^\ell e^{-i\frac{2\pi k\ell}{N_{UF}M}} \sum_{m=-\Delta}^{\Delta} \Re\left(G_\ell(m)\right) e^{i\frac{2\pi km}{M}}. \tag{20}$$

Neglecting the effect of multipath (delay spread) and noise, the complete $N_R \times 1$ received signal is

$$\boldsymbol{r}(k) = \boldsymbol{H}\times \boldsymbol{s}(k), \tag{21}$$

where $\boldsymbol{H}\in\mathbb{C}^{N_R\times U}$ is the MIMO channel matrix, and $\boldsymbol{s}(k)$ is the baseband signal defined in (1). Substituting (1) in (21), we get

$$\boldsymbol{r}(k) = \boldsymbol{H}\times \sum_{n'=-\infty}^{+\infty} g\left(k-n'\frac{M}{2}\right)\boldsymbol{x}_{\boldsymbol{n}'}(k). \tag{22}$$

By substituting (22) in (19), the ℓ^{th} AFB output number will be

$$\boldsymbol{Y}_{\boldsymbol{n}}(m,\ell) = \sum_{s=\mathbf{0}}^{\mathrm{N_{UF}}-1}\sum_{k=0}^{M-1}\sum_{n'=-\infty}^{+\infty} g_\ell(k)g(p'_{n-n'})\boldsymbol{x}_{\boldsymbol{n}'}(p'_n)\frac{P}{e^{-i\frac{2\pi k\ell}{N_{UF}M}}}. \tag{23}$$

[1]Indicates a constant SIR value, confirming the support of asynchronous communication.

However, due to the time localization of the NPR1 PF, interference is limited to only neighboring FBMC symbols. Hence, by defining $q = (n - n'), \in [-1, 1]$, (23) becomes

$$\boldsymbol{Y}_n(m,\ell) = \sum_{s=0}^{N_{UF}-1} \sum_{q=-1}^{1} \sum_{k=0}^{M-1} g_\ell(k) g(p'_q) \boldsymbol{x}_{n-q}(p'_n) \frac{P}{e^{-i\frac{2\pi k\ell}{N_{UF}M}}}. \tag{24}$$

In fact, the third sum in the previous equation is nothing but the FFT of the inner term. Moreover, since the Fourier transform of a product is the circular convolution of the corresponding transforms, then (24) can be written as

$$\begin{aligned}\boldsymbol{Y}_n(m,l) &= \sum_{s=0}^{N_{UF}-1} \sum_{q=-1}^{1} F_{g_{l,s}}(m,q) \otimes \boldsymbol{X_{n-q}}(m) \\ &= \sum_{s=\mathbf{0}}^{N_{UF}-1} \sum_{q=-1}^{1} \sum_{p=-\frac{M}{2}}^{\frac{M}{2}-1} F_{g_{l,s}}\left(p, q\frac{M}{2}\right) \boldsymbol{X_{n-q}}(m-p),\end{aligned} \tag{25}$$

where $\otimes$ denotes a circular convolution, and

$$\boldsymbol{X_{n-q}}(m-p) = \boldsymbol{a_{n-q}}(m-p)\phi_{\boldsymbol{n-q}}(m-p), \tag{26}$$

along with

$$F_{g_{\ell,s}}(p,q) = \sum_{k=0}^{M-1} g_\ell(k) g\left(k + Ms + q\right) e^{-i\frac{2\pi s\ell}{N_{UF}}} e^{-i\frac{2\pi kp}{M}}. \tag{27}$$

Substituting (26) in (25), we get

$$\begin{aligned}\boldsymbol{Y_n}(m,\ell) = \sum_{s=\mathbf{0}}^{N_{UF}-1} \sum_{(p,q)\in\Omega} F_{g_{\ell,s}}\left(p, q\frac{M}{2}\right) \boldsymbol{a_{n-q}}(m-p) \\ \times \phi_{\boldsymbol{n-q}}(m-p),\end{aligned} \tag{28}$$

where $\Omega = \left[-\frac{M}{2}, \frac{M}{2} - 1\right] \times [-1, 1]$. Finally, by developing (8), the estimated data symbols $\widehat{\boldsymbol{a_n}}(m)$ of all users will be

$$\begin{aligned}\widehat{\boldsymbol{a_n}}(m) &= \Re\left[\phi_n^*(m) \sum_{\ell=0}^{N_{UF}-1} \boldsymbol{Y}_n(m,\ell)\right] \\ &= \Re\Bigg[\sum_{(\ell,s)\in\Omega_1} \sum_{(p,q)\in\Omega} \mathrm{i}^{-\boldsymbol{q}-\boldsymbol{p}} F_{g_{\ell,s}}\left(p, q\frac{M}{2}\right) \times \\ &\quad \boldsymbol{a_{n-q}}(m-p)\Bigg],\end{aligned} \tag{29}$$

where $\Omega_1 = [0, N_{UF} - 1] \times [0, N_{UF} - 1]$. Actually, in the presence of CFO, the previous equation can be written as

$$\begin{aligned}\widehat{\boldsymbol{a_n}}(m) &= \Re\Bigg[\boldsymbol{C_{CPE}}(n)\phi_n^*(m) \sum_{(\ell,s)\in\Omega_1} \sum_{(p,q)\in\Omega} g_\ell(k) \times \\ &\quad g(p'_q)\boldsymbol{x}_{n-q}(p'_n) e^{-i\frac{2\pi s\ell}{N_{UF}}} e^{-i\frac{2\pi k(m+r)}{N_{UF}}}\Bigg] \\ &= \Re\Bigg[\sum_{(l,s)\in\Omega_1} \sum_{(p,q)\in\Omega} \mathrm{i}^{-\boldsymbol{q}-\boldsymbol{p}} F_{g_{l,s}}\left(p+r, q\frac{M}{2}\right) \times \\ &\quad \boldsymbol{a_{n-q}}(m-p)\Bigg],\end{aligned} \tag{30}$$

where r is the CFO normalized to the subcarrier spacing Δf, and $\boldsymbol{C_{CPE}}(n) = e^{j\pi nr}$ is the common phase error (CPE) compensation term introduced by CFO.

Keeping in mind that $\boldsymbol{a_n}(m)$ are independent and identically distributed random variables with zero mean, then the SIR expression arising from a CFO of r is

$$\begin{aligned}&\mathbf{SIR_{OS,CFO}}(r) = \\ &\frac{\left(\sum_{(\ell,s)\in\Omega_1} \Re\Big(F_{g_{\ell,s}}(r,0)\Big)\right)^2}{\sum_{(\ell,s)\in\Omega_1} \sum_{(p,q)\in\Omega^0} \Re\Big(\mathbf{i}^{-q-p} F_{g_{\ell,s}}\left(r, q\frac{M}{2}\right)\Big)^2},\end{aligned} \tag{31}$$

where Ω_0 is $\Omega/(0,0)$.

b) OSB Receiver: Through similar development, equation (11) can be adapted to obtain the expression of the recovered PAM symbols $\widehat{\boldsymbol{a_{b,n}}}$ of all users in a block $\boldsymbol{b}$ when a CFO r is applied, as follows

$$\begin{aligned}\widehat{\boldsymbol{a_{b,n}}}(m) = \Re\Bigg[\sum_{(l,s)\in\Omega_1} \sum_{(p,n)\in\Omega_2} i^{-p} F_{g_{l,s}}\left(p+r, n\frac{M}{2}\right) \times \\ (-1)^{n(m-p)} \boldsymbol{a_{b,n}}(m-p)\Bigg],\end{aligned} \tag{32}$$

where $\Omega_2 = \left[-\frac{M}{2}, \frac{M}{2} - 1\right] \times [0, N_s - 1]$. Hence, the SIR expression arising from a CFO of r for the OSB receiver becomes:

$$\begin{aligned}&\mathbf{SIR_{OSB,CFO}}(r) = \\ &\frac{\left(\sum_{(l,s)\in\Omega_1} \sum_{n=0}^{Ns-1} \Re\Big(F_{g_{l,s}}\left(r, n\frac{M}{2}\right)\Big)\right)^2}{\sum_{(l,s)\in\Omega_1} \sum_{(p,n)\in\Omega_2^0} \Re\Big(\mathbf{i}^{-p} F_{g_{l,s}}\left(r, n\frac{M}{2}\right)\Big)^2}\end{aligned} \tag{33}$$

B. Analytical SIR expression in the presence of TO

a) OS Receiver: The robustness of the $\mathrm{OS}_{N_{UF}}$-FBMC receiver to TO can be proved analytically by considering the time domain equalizer in [27] with MU-mMIMO and disregarding multipath. Hence, the frequency domain equalized signal for all users is

$$\underbrace{\boldsymbol{X_n}(m)}_{\in\mathbb{C}^{U\times 1}} = \underbrace{\boldsymbol{C_n}(m)}_{\in\mathbb{C}^{U\times N_R}} \times \sum_{k=0}^{N-1} \underbrace{\boldsymbol{r}(k + n\frac{M}{2})}_{\in\mathbb{C}^{N_R\times 1}} e^{-i\frac{2\pi km}{N}}. \tag{34}$$

Adapting the previous equation in the presence of TO of l_d samples, we have

$$\begin{aligned}\boldsymbol{X}_n(m) &= \boldsymbol{C}_n(m)\boldsymbol{C_{TO}}(m) \sum_{k=0}^{N-1} \boldsymbol{r}\left(k + l_d + n\frac{M}{2}\right) e^{-i\frac{2nkm}{N}} \\ &= \boldsymbol{C}_n(m) \times \sum_{k=0}^{N-1} \boldsymbol{r}\left(k + l_d + n\frac{M}{2}\right) e^{-i\frac{2n(k+l_d)m}{N}},\end{aligned} \tag{35}$$

where $\boldsymbol{C_{TO}}(m) = e^{-i\frac{2\pi m l_d}{N'}}$ and $N' = N_{UF}M$. By applying the following change of variable $k = k + l_d$, we have

$$\boldsymbol{X}_n(m) = \boldsymbol{C}_n(m) \times \sum_{k=l_d}^{N+l_d-1} \boldsymbol{r}\left(k + n\frac{M}{2}\right) e^{-i\frac{2nkm}{N}}. \quad (36)$$

Suppose that $l_d > 0$, then (36) becomes

$$\boldsymbol{X_n}(m) = \boldsymbol{C_n}(m) \times \left[\sum_{k=0}^{N-1} \boldsymbol{r}\left(k + n\frac{M}{2}\right) e^{-i\frac{2nkm}{N}} + \sum_{k=0}^{l_d-1} \left(\boldsymbol{r}\left(k + N + n\frac{M}{2}\right) - \boldsymbol{r}\left(k + n\frac{M}{2}\right)\right) \times e^{-i\frac{2nkm}{N}}\right]. \quad (37)$$

At the output of the OS time-domain equalizer, we have

$$\begin{aligned}\boldsymbol{x_n}(k) &= \sum_{m=0}^{N-1} \boldsymbol{X_n}(m) e^{i\frac{2m\pi(k+l_0)}{N}} \\ &= \boldsymbol{c_n}(k) \times A,\end{aligned} \quad (38)$$

where $k \in [0, M-1]$, $l_0 = \frac{(N_{UF}-1)M}{2}$,

$$A = \left[\boldsymbol{r}\left(k + l_0 + n\frac{M}{2}\right) + \boldsymbol{\Pi}_{l_d}(k + l_0) \times \left(\boldsymbol{r}\left(k + N + l_0 + \frac{M}{2}n\right) - \boldsymbol{r}\left(k + l_0 + \frac{M}{2}n\right)\right)\right], \quad (39)$$

and

$$\Pi_x(k) = \begin{cases} k, & k < x \text{ and } x > 0 \\ 0, & k \geq x \text{ or } x \leq 0 \end{cases}. \quad (40)$$

By making another change of variable $k = k + l_0$, (39) becomes

$$\boldsymbol{x_n}(k) = \boldsymbol{c_n}(k) \times \left[\boldsymbol{r}\left(k + n\frac{M}{2}\right) + \underbrace{\boldsymbol{I}(k)}_{\text{Interfering signal}}\right], \quad (41)$$

where $k \in [l_0, l_0 + M - 1]$, and

$$\boldsymbol{I}(k) = \boldsymbol{\Pi}_{l_d}(k)\left[\boldsymbol{r}\left(k + N + \frac{M}{2}n\right) - \boldsymbol{r}\left(k + \frac{M}{2}n\right)\right]. \quad (42)$$

The lowest possible value of l_0 is $\frac{M}{2}$ for $N_{UF} = 2$. Moreover, when $l_d < l_0$, then $\boldsymbol{\Pi}_{l_d}(k) = 0$. When $-l_0 < l_d < 0$, the same conclusion can be obtained through a similar development. Hence, this confirms that the OS$_{N_{UF}}$-FBMC receiver is insensitive to a TO lower than 50% of the symbol duration for all $N_{UF} \geq 2$.

b) OSB Receiver: Let's also consider the OS time domain equalizer in [27] but applied to a block of FBMC symbols with mMIMO. Adapting (34) but with a block $\boldsymbol{b}$, the frequency domain equalized signal for a block $\boldsymbol{b}$ and all users will be

$$\underbrace{\boldsymbol{X_{b,n}}(m)}_{\in \mathbb{C}^{U\times 1}} = \underbrace{\boldsymbol{C_{b,n}}(m)}_{\in \mathbb{C}^{U\times N_R}} \times \sum_{k=0}^{N-1} \underbrace{\boldsymbol{r_b}(k)}_{\in \mathbb{C}^{N_R\times 1}} e^{-i\frac{2\pi km}{N}}. \quad (43)$$

Actually, in the presence of TO for an OSB receiver, only the first or last FBMC symbol is affected by interference. Hence, adapting the previous equation in the presence of TO and by considering only the first FBMC symbol ($n = 0$), we have

$$\begin{aligned}\boldsymbol{X_{b,0}}(m) &= \boldsymbol{C_{b,0}}(m) \times \boldsymbol{C_{TO}}(m) \sum_{k=0}^{N-1} \boldsymbol{r_b}(k + l_d) e^{-i\frac{2\pi km}{N}} \\ &= \boldsymbol{C_{b,0}}(m) \times \sum_{k=0}^{N-1} \boldsymbol{r_b}(k + l_d) e^{-i\frac{2\pi(k+l_d)m}{N}}.\end{aligned} \quad (44)$$

By neglecting the effect of multipath and noise, substituting the value of $\boldsymbol{r_b}(k)$ in (44), and by applying the change of variable $k = k + l_d$, we have

$$\underbrace{\boldsymbol{X_{b,0}}(m)}_{\in \mathbb{C}^{U\times 1}} = \underbrace{\boldsymbol{C_{b,0}}(m)}_{\in \mathbb{C}^{U\times N_R}} \times \sum_{k=l_d}^{N+l_d-1} \underbrace{\boldsymbol{H}}_{\in \mathbb{C}^{N_R\times U}} \times \underbrace{\boldsymbol{s_b}(k)}_{\in \mathbb{C}^{U\times 1}} e^{-i\frac{2\pi km}{N}}. \quad (45)$$

Similarly as before, if $l_d > 0$, then (45) becomes

$$\boldsymbol{X_{b,0}}(m) = \left[\sum_{k=0}^{N-1} \boldsymbol{s_b}(k) e^{-i\frac{2\pi km}{N}} + \sum_{k=N}^{N+l_d-1} \boldsymbol{s_b}(k) e^{-i\frac{2\pi km}{N}} - \sum_{k=0}^{l_d-1} \boldsymbol{s_b}(k) e^{-i\frac{2\pi km}{N}}\right]. \quad (46)$$

At the output of the OS time domain equalizer applied to a block $\boldsymbol{b}$ we have

$$\boldsymbol{x_{b,0}}(k) = \left[\underbrace{\boldsymbol{s_b}(k)}_{\text{Transmitted signal}} + \underbrace{\boldsymbol{\Pi_{l_d}}(k)\boldsymbol{s_b}(k+N) - \boldsymbol{\Pi_{l_d}}(k)\boldsymbol{s_b}(k)}_{\text{Interfering signal } \boldsymbol{I}_b(k)}\right], \quad (47)$$

where $\boldsymbol{\Pi_{l_d}}(k)$ is defined in (40).The interfering term can be expressed as

$$\boldsymbol{I_b}(k) = \boldsymbol{\Pi_{l_d}}(k) g(k) \sum_{m=0}^{M-1} \boldsymbol{\phi_0}(m) \boldsymbol{A'}_m e^{i\frac{2\pi km}{N}}, \quad (48)$$

where $\boldsymbol{A'}_m = \boldsymbol{a_{b+1,0}}(m) - \boldsymbol{a_{b,0}}(m)$, $\boldsymbol{a_{b+1,0}}(m)$ and $\boldsymbol{a_{b,0}}(m)$ are the transmitted data symbols of distinct users at the first FBMC symbol of blocks $\boldsymbol{b+1}$ and $\boldsymbol{b}$ respectively. Hence, at the output of AFB we have

$$\boldsymbol{I_b}(m) = \sum_{p=-\frac{M}{2}}^{\frac{M}{2}-1} F_{g_{l_d}}(p) \boldsymbol{\phi_0}(m-p) \boldsymbol{A'}_{m-p}, \quad (49)$$

where

$$F_{g_{l_d}}(p) = \sum_{k=0}^{M-1} \Pi_{l_d}(k) g^2(k) e^{-i\frac{2\pi km}{N}}. \quad (50)$$

Then, after OQAM demodulation, the interference term at the output of the FBMC receiver $\{\boldsymbol{D_b}(m) = \mathrm{R}\left(\boldsymbol{\phi_0^*}(m)\boldsymbol{I_b}(m)\right)\}$ can be expressed as

$$\boldsymbol{D_b}(m) = \Re\left(\sum_{p=-\frac{M}{2}}^{\frac{M}{2}-1} i^{-p} F_{g_{\boldsymbol{l_d}}}(p) \boldsymbol{A'}_{m-p}\right). \quad (51)$$

Recall that interference is only introduced at the first FBMC symbol in a block $\boldsymbol{b}$, then

$$\widehat{a_{b,n}}(m) = a_{b,n}(m) + \underbrace{\boldsymbol{D_b}(m)}_{\text{Only for n=0}} + \boldsymbol{T_{b,n}}(m), \tag{52}$$

where $\boldsymbol{T_{b,n}}(m)$ represents the interference induced by truncation.
Finally, the SIR expression arising from a TO of l_d samples for the OSB-FBMC receiver can be expressed as

$$\mathbf{SIR}_{\mathrm{OSB}}(l_d) \approx \frac{E\left(\mathbf{a}^2_{\mathbf{b},\mathbf{n}}(m)\right)}{\frac{1}{N_s}E\left(\boldsymbol{D_b}(m)^2\right) + E\left(\boldsymbol{T_{b,n}}(m)^2\right)}. \tag{53}$$

where the expected value of $\boldsymbol{T_{b,n}}(m)$ can be written as

$$E\left(\boldsymbol{T_{b,n}}(m)\right) = \sum_{(p,q)\in\Omega^0} \Re\left[i^{p+q}F_{g,\tilde{g}}\left(p, q\frac{M}{2}\right)\right]^2.$$
$$F_{g,\tilde{g}}(p,q) = \sum_{k=0}^{M-1} g(k+q)\tilde{g}(k)e^{-i2\pi\frac{pk}{M}} \tag{54}$$

with $\tilde{g}(k) = \sum_{l=-\Delta}^{\Delta} G(l)e^{i2\pi\frac{kl}{M}}$.
Since the data $\boldsymbol{a_{b,n}}(m)$ of the users are independent and identically distributed random variables of mean 0 and variance σ_d^2 then

$$E\left(\boldsymbol{D_b}(m)^2\right) = 2\sigma_d^2 \sum_{p=-\frac{M}{2}}^{\frac{M}{2}-1} \mathrm{R}\left(i^{-p}F_{g_{l_d}}(p)\right)^2. \tag{55}$$

Hence, (53) becomes

$$\mathbf{SIR}_{\mathrm{TO,OSB}}(l_d) \approx \frac{\sigma_d^2}{\frac{1}{N_s}2\sigma_d^2\sum_{p=-\frac{M}{2}}^{\frac{M}{2}-1}\mathrm{R}\left(i^{-p}F_{g_{l_d}}(p)\right)^2 + E\left(\boldsymbol{T_{b,n}}(m)^2\right)}. \tag{56}$$

C. Analysis of the asymptotic behavior

When the number of antennas at the BS tends to infinity, the channel distortions tend to average out. As a result, the SINR saturates at a predetermined level depending on system parameters. This establishes an upper limit for the SINR performance of the system. We will determine its analytical expression. For that, we neglect the effect of noise, because the noise contribution fades away in an asymptotic regime. By adapting equations (1) and (2), in the presence of multipath and absence of noise the received signal at the j^{th} BS antenna can be expressed as

$$\begin{aligned} r_j(k) &= \sum_{l'=0}^{L-1}\sum_{u=0}^{U-1}\sum_{n'=-\infty}^{+\infty}\sum_{m'=0}^{M-1} a_{n',m'}g_{m'}(k - n'\frac{M}{2} - l') \\ &\quad\times \phi_{n'}(m')h_{j,u}(l') \\ &= \sum_{u=0}^{U-1}\sum_{n'=-\infty}^{+\infty}\sum_{m'=0}^{M-1} a_{n',m'}g_{m'}(k - n'\frac{M}{2}) \\ &\quad\times \phi_{n'}(m') * h_{j,u}(k), \end{aligned} \tag{57}$$

where $(*)$ denotes a linear convolution, $h_{j,u}(l')$ is the channel impulse response between a user u and the j^{th} BS with $l' \in [0, L-1]$, L is the total number of paths, and $g_m(k) = g(k)e^{j\frac{2\pi mk}{M}}$ is the PF modulated to center frequency of subcarrier m. Equivalently, for N_R antennas the previous equation can be written as

$$\boldsymbol{r}(k) = \sum_{n'=-\infty}^{\infty}\sum_{m'=0}^{M-1} \phi_{n'}(m') \times P' \times \boldsymbol{a_{n',m'}}, \tag{58}$$

where

$$P' = \begin{bmatrix} P_{1,1}(k) & \dots & P_{1,U}(k) \\ \vdots & \ddots & \vdots \\ P_{N_R,1}(k) & \dots & P_{N_R,U}(k) \end{bmatrix}, \tag{59}$$

$P_{j,u}(k) = g_{m'}(k - n'\frac{M}{2}) * h_{j,u}(k)$, and $\boldsymbol{a_{n',m'}} \in \mathbb{C}^{U\times 1}$ is a vector containing all transmitted data symbols of the users at subcarrier m' and at time index n'. Adapting (19) we have

$$\begin{aligned} \boldsymbol{Y}_n(m,\ell) = \boldsymbol{C_n(m)} \times \sum_{s=0}^{N_{UF}-1}\Bigg(\sum_{n'=-\infty}^{\infty}\sum_{m'=0}^{M-1} H_{mm',nn'} \\ \times \boldsymbol{a_{n',m'}}\phi_{n'}(m')\Bigg), \end{aligned} \tag{60}$$

where $\boldsymbol{H_{mm',nn'}}$ is an $N_R \times U$ matrix that can be expressed as

$$\boldsymbol{H_{mm',nn'}} = \begin{bmatrix} H^{1,1}_{mm',nn'} & \dots & H^{1,U}_{mm',nn'} \\ \vdots & \ddots & \vdots \\ H^{N_R,1}_{mm',nn'} & \dots & H^{N_R,U}_{mm',nn'} \end{bmatrix}, \tag{61}$$

along with

$$\begin{aligned} H^{j,u}_{mm',nn'} &= g_{m'}(p'_{n-n'}) * h_{j,u}(p'_n) * g_{m,\ell}(k), \\ g_{m,\ell}(k) &= (-1)^\ell e^{-i\frac{2\pi s\ell}{N_{UF}}}\sum_{k=0}^{M-1} g(k)e^{-i\frac{2\pi km}{M}}. \end{aligned} \tag{62}$$

Similarly, interference is limited to only neighboring FBMC symbols. Hence, (60) becomes

$$\begin{aligned} \boldsymbol{Y}_n(m,\ell) = \boldsymbol{C_n(m)}\times \\ \sum_{s=0}^{N_{UF}-1}\Bigg(\sum_{(q,m')\in\Omega_3} H_{mm',n(n-q)} \\ \times \boldsymbol{a_{n-q,m'}}\phi_{n-q}(m')\Bigg), \end{aligned} \tag{63}$$

where $\Omega_3 = [-1,1][0, M-1]$. Adapting equations (7) and (8), the estimated data symbols of the users will be

$$\begin{aligned} \widehat{\boldsymbol{a}}_{n,m} &= \Bigg[\sum_{(\ell,s)\in\Omega_1} \boldsymbol{C_n(m)} \times \sum_{(q,m')\in\Omega_3} H_{mm',n(n-q)}\times \\ &\quad \boldsymbol{a_{n-q,m'}}\phi_{n-q}(m')\phi^*_n(m)\Bigg] \\ &= \mathrm{R}\Bigg[\sum_{(\ell,s)\in\Omega_1}\sum_{(q,m')\in\Omega_3} G_{mm',n(n-q)}\boldsymbol{a}_{n-q,m'}\times \\ &\quad \phi_{n-q}(m')\phi^*_n(m)\Bigg], \end{aligned} \tag{64}$$

where $\boldsymbol{G_{mm',nn(n-q)}}$ is an $U \times U$ matrix defined as $\boldsymbol{C_n(m)H_{mm',n(n-q)}}$.

In order to compute the elements of $\boldsymbol{G_{mm',n(n-q)}}$ in the asymptotic regime, let us recall the law of large numbers in probability theory. Let a and b be two random vectors each with n identically independent elements. As a result of the law of large numbers (i.e. as n tends to infinity), the random variable $\frac{1}{n}a^H b$ will almost converge to $Cab = E[a_i^* b_i]$, with $i = 1, ..., n$.

Similarly, in our case when the number of antennas at the BS N_R tends to infinity, the law of large numbers can be used to compute the elements of $\boldsymbol{G_{mm',n(n-q)}}$.

The ZF equalizer matrix is defined as $\left(\boldsymbol{H_m^H H_m}\right)^{-1}\boldsymbol{H_m^H}$, where $\boldsymbol{H_m}$ is the matrix of channel coefficients at the center of the m^{th} subcarrier (i.e. $H_m^{j,u} = \sum_{l'=0}^{L-1} h_{j,u}(l')e^{-j\frac{2\pi m l'}{M}}$).

Note that $\left(\frac{1}{N_R}\boldsymbol{H_m^H H_m}\right)^{-1}$ tends to $\boldsymbol{I_U}$ as N_R tends to infinity. Then according to the previously introduced law of large numbers, the elements in $\boldsymbol{G_{mm',n(n-q)}}$ will converge to

$$G^{u,u'}_{mm',n(n-q)} \rightarrow \mathbb{E}\left\{\left(H_m^{j,u}\right)^* H^{j,u'}_{mm',n(n-q)}\right\}. \tag{65}$$

Substituting the value of $H^{j,u}_{mm',n(n-q)}$, then (65) will be

$$G^{u,u'}_{mm',n(n-q)} \rightarrow g_{m'}(p'_q) * \mathbb{E}\left\{\left(H_m^{j,u}\right)^* h_{j,u'}(p'_n)\right\} * g_{m,\ell}(k), \tag{66}$$

where

$$\begin{aligned}\mathbb{E}\left\{\left(H_m^{j,u}\right)^* h_{j,u}(p'_n)\right\} &= \sum_{l'=0}^{L-1}\mathbb{E}\left\{h^*_{j,u}(l')h_{j,u'}(p'_n)\right\}e^{j\frac{2\pi l' m}{M}} \\ &= \rho_u(p'_n)e^{j\frac{2\pi p'_n m}{M}}\delta^{uu'} \\ &= \rho_{m,u}(p'_n)\delta^{uu'},\end{aligned} \tag{67}$$

where $\rho_{m,u}(l') = \rho_u(l')e^{j\frac{2\pi l' m}{M}}$ is the channel power delay profile (PDP) of the u^{th} user modulated to the m^{th} subcarrier.

The left-hand side term of (67) tends to zero when $u \neq u'$. This is due to the fact that the effect of multi-user interference vanishes as the number of antennas at the BS tends to infinity. However, residual self-interference is experienced by the user when $u = u'$. Therefore, for a given user u and starting from (66), the equivalent channel impulse response (CIR) between the transmitted data symbols at subcarrier m' and the received ones at subcarrier m tends to

$$g_{m'}(p'_q) * \rho_{m,u}(p'_n) * g_{m,\ell}(k). \tag{68}$$

As a result, the SINR for a user u saturates to

$$\mathbf{SINR}^u_{m,n} \rightarrow \frac{\sum_{(l,s)\in\Omega_1}\Re^2\left\{G_{mm,nn}\right\}}{\sum_{(l,s)\in\Omega_1}\sum_{(m',q)\in\Omega\neq(m,0)}\Re^2\left\{G_{mm',n(n-q)}\right\}}. \tag{69}$$

D. Summary and direct application

Depending on the used OS-based receivers, a step-by-step guide for the direct application of the derived SIR expressions in the presence of CFO and TO is provided in Table I.

Parameters	Value
Carrier frequency	3.5 GHz
Cyclic prefix	36 samples
Channel model	'3GPP_3D_Uma-NLOS' '3GPP-38.901-Rma'
Total number of subcarriers	512 subcarriers
Sub-band size N_c	300 subcarriers
Number of UE	4
BS height	25 m
Number of BS antennas	64
Number of vertical/horizontal panels	2/1
Vertical and horizontal antennas spacing	42.85 mm

TABLE II: Simulation Parameters

V. Simulation Setup

In this section, we describe the used filtered discrete channel model, as well as the simulation tool and the antenna array structure.

A. Channel model

A discrete multipath channel model in rapidly changing environments features a variable number of paths as well as variable path gains. However, for reference channels, the number of discrete components can be considered to be constant. Consider a channel model with L paths; then the channel impulse response $h_u(k,t)$ for antenna k and user u is given by

$$h_u(k,t) = \sum_{l'=1}^{L} b_{l,u}(k)\delta(t - \tau_{l',u}(k)), \tag{70}$$

where k is the antenna index, l' is the path index, u is the user index, $\tau_{l',u}(k)$ is the path delay, and $b_{l',u}(k)$ is the path complex amplitude.

According to [28], it is advantageous to band limit the channel by design to achieve better simulation properties when the differential delays are small relative to the simulation sampling time T_s or are not integer multiples of T_s. Hence, the channel impulse response is band-limited using an ideal rectangular filter. Thus, the filtered discrete channel impulse response is given by

$$\tilde{h}(k,n) = \sum_{l'=1}^{L} b_{l',u}(k)sinc\Big(\frac{\tau_{l',u}(k)}{T_s} - n\Big), \tag{71}$$

where $-N_1 \leq n \leq N_2$, N_1 and N_2 are the tap indices chosen such that $\tilde{h}(k,n)$ is small when n is less than N_1 or larger than N_2, and $sinc(x) = sin(x)/x$ [28]. In our simulations, the tap indices are chosen such that the value of $\tilde{h}(k,n)$ at the relevant tap indices is larger by at least 1% of its maximum.

According to [29], the delay value may be considered to be independent of the antenna index k, i.e. $\tau_{m,u}(k) = \tau_{m,u}$ if the maximum distance between antenna elements divided by the speed of light $(d_{\max}/c)$ is much smaller than $\frac{1}{B}$ value, where B is the transmission bandwidth.

B. Simulation tool

QuaDRiGa (QUAsi Deterministic RadIo channel GenerAtor) [30] was developed to enable the modeling of MIMO

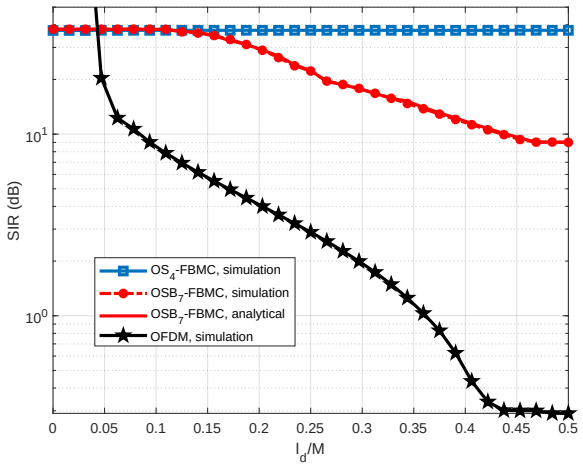

Fig. 2: SIR evaluation for the OS-based receivers in the presence of TOs with 4 users and 64 receiving antennas.

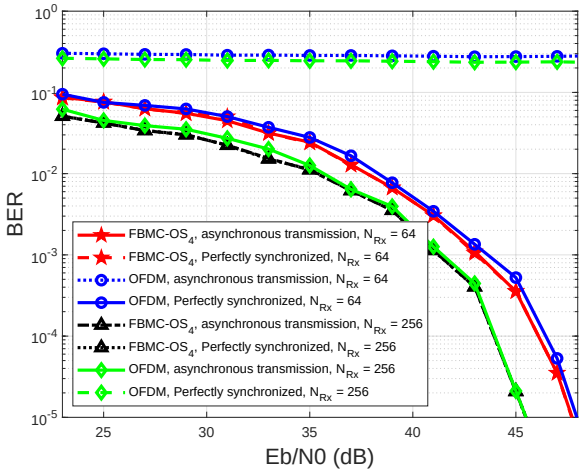

Fig. 3: Comparison of BER performance for asynchronous transmissions over the 5G QuaDRiGa channel under the 3GPP-38.901-Rma scenario with 4 users, 64 and 256 receiving antennas.

radio channels for specific network configurations. QuaDRiGa incorporates a set of characteristics developed in the Spatial Channel Model (SCM) [31] and WINNER channel models [32], as well as modeling methodologies to enable quasi-deterministic multi-link tracking of the movements of users in changing environments. For our simulations, QuaDRiGa is used to generate realistic radio channels. Chosen parameters follow the 5G standard [10] with cross-polarized 64 antennas at the BS.

C. Antenna array structure

For the 3D-Uma-NLOS and 3GPP-38.901-Rma models of the 5G QuaDRiGa channel, the antenna array at the BS is 25 meters high and consists of two co-located rectangular sub-arrays, each with 32 antennas as in [33]. Each sub-array is designated by (N_V, N_H, N_P), where $N_H = 2$ represents the number of columns, $N_V = 8$ represents the number of antenna elements with the same polarization in each column, and $N_P = 2$ represents the number of polarization as proposed in [34]. Therefore, with $N_{gV} = 2$ vertical antenna panels, the number of antennas is calculated as $\{N_R = N_{gV} N_V N_H N_P = 64\}$. With λ being the carrier wavelength, the 2 antenna panels are spaced in the vertical direction with a spacing of $d_{gV} = \lambda$, and the antenna units placed inside each panel are uniformly spaced in the horizontal and vertical directions with a spacing of $d_H = 0.5\lambda$ and $d_V = 0.5\lambda$ respectively, where $\lambda = 85.7$ mm. Specific simulation parameters, aligned with the typical 3GPP 5G standard [10], are summarized in Table II.

D. Simulation parameters

The number of non-truncated filter coefficients is set to $N_G = 7$ for an SIR of 55 dB [17]. For the OS-FBMC based receivers, the up-sampling factor used for the OS technique is set to $N_{UF} = 4$ which is a good compromise between system performance and complexity. The number of FBMC symbols in a block N_s for the OSB-FBMC receiver is set to 7. This is reflected by the OS$_4$-FBMC and OSB$_7$-FBMC receiver notations. Considered conStellations are 4 and 16-QAM. Furthermore, the channel state information (CSI) is assumed to be perfectly estimated at the receiver side.

E. Applying Analytical derivations: A Practical Example

In this section, we provide an application example for using the analytical derivations by applying the step-by-step guide outlined in Table I. For instance, consider a TO value l_d, corresponding to 44% of the symbol duration. Using the simulation parameters presented in the previous section, we evaluate equation (56) using equation (51). Consequently, using equation (50), the expected value of equation (51) yields approximately 0.35. The truncation-related interference is computed using equation (54), yielding an approximate value of 3.55×10^{-6}. Therefore, the SIR value corresponding to this l_d is approximately 10 dB. This same methodology can be applied systematically to compute other expressions of SIR.

VI. Performance over static channels

In this section the bit-error rate (BER) and SIR performance of the OS-based FBMC receivers is compared to OFDM on the 5G QuaDRiGa static channel under the effect of TO impairments and in an asynchronous transmission scenario.

A. Timing offsets

TO impairments occur when the processing windows at the transmitter and receiver are not aligned in time, yielding residual interference. Therefore, timing synchronization algorithms must be employed. However, in order to save power in the future beyond 5G systems, it is desirable to consider relaxed synchronization and asynchronous communications. As a result, each subcarrier will experience a linear phase rotation (LPR). In fact, the latter can be completely compensated for

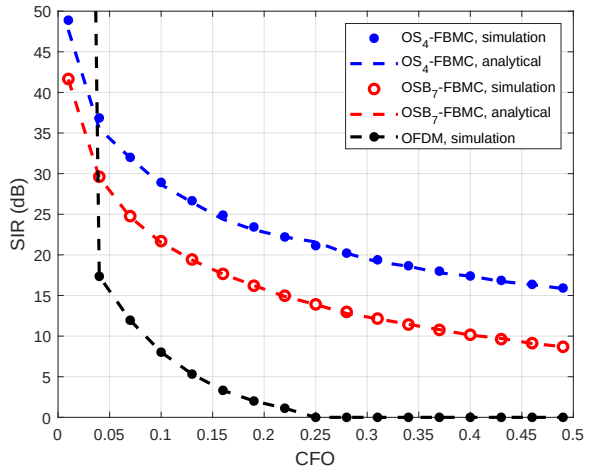

Fig. 4: SIR evaluation for the OS-based receivers in the presence of CFO.

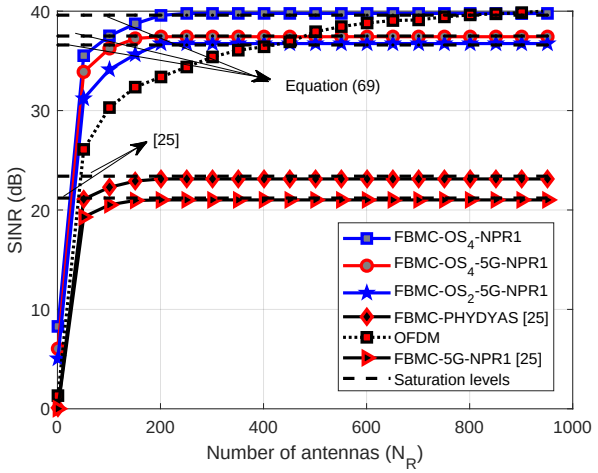

Fig. 5: SINR saturation level comparison for different FBMC receivers considering different channels with 4 users and 64 receiving antennas.

by FBMC associated with the proposed receivers directly after channel estimation and equalization. Therefore, if l_d is the TO in samples, then the frequency domain compensation term is expressed as $C_{TO}(m) = e^{-i\frac{2\pi m l_d}{N'}}$ where $N' = M$ for OFDM, and $N' = N_{UF}M$ for the OS-based FBMC receivers. For our simulations, the receiver is considered perfectly time-aligned when the first sample processed by the FFT is the sample located at the middle of the CP length, allowing for both positive and negative TO values.

In order to validate the robustness of the OS receivers to TO impairments, we plot in Figure 2 the SIR obtained by simulation for the OS_4-FBMC, and the OSB_7-FBMC receivers, as well as the SIR determined by evaluating (56). As depicted in the figure, the SIR of the OS_4-FBMC receiver is unaffected by TO, supporting the analytical study performed in Section IV-B. Unlike the OS_4-FBMC receiver, the OSB_7-FBMC receiver, cannot support any TO less than half the symbol duration, as illustrated and validated analytically in the same figure. In fact, according to Figure 2, the SIR of the OSB_7-FBMC receiver achieves a constant value up to a TO of 12% of the symbol duration, showing that the introduced interference is limited. The SIR gradually decreases as the TO value increases showing that the introduced interference is no longer limited. Finally, OFDM is free from any interference when $l_d < \frac{L_{CP}}{2}$, but it is clearly outperformed by FBMC associated to the OS-based receiver for larger TO values.

B. Asynchronous communication

The 5G network is designed to accommodate new and highly demanding scenarios such as massive machine communications, which require asynchronous communication. The latter is considered a cornerstone for grant-free spectrum and massive access since it allows each user to transmit at an independent time reference without the need for time synchronization among all scheduled users. However, this can lead to time misalignment between users, which may vary within the same subband. To investigate the performance of the FBMC-OS_4 receiver for asynchronous communications compared to OFDM, we consider 4 users transmitting asynchronously in time and then evaluate the BER over the 5G QuaDRiGa channel under the 3GPP-38.901-Rma scenario with a cell radius of 10 km, as shown in Figure 3. Starting with 64 receiving antennas, both receivers show similar BER performance when the users are perfectly synchronized, but when users send signals at independent time references within the same band, OFDM suffers from an irreducible error floor, while the BER performance for the FBMC-OS_4 receiver remains unaffected, showing the same performance as perfectly synchronized users. Similar conclusions can be drawn when the number of receiving antennas is increased to 256. Despite this increase, the OFDM receiver still suffers from an irreducible error floor as depicted in the same figure. This confirms the support of the FBMC-OS receiver for asynchronous communications.

VII. Performance over non-static channels

OFDM is well-known for being extremely sensitive to CFOs induced by Doppler spread/shift [7]. In fact, the effect of Doppler spread/shift on system performance is worse in MU-mMIMO systems since the potential gains of mMIMO are heavily reliant on the accuracy of frequency synchronization. Hence, in this section the SIR performance of the OS-based FBMC receivers is compared to OFDM in the presence of CFOs.

A. Carrier frequency offset

CFOs arises when the local oscillators of the transmitter and receiver are out of phase, which can happen more frequently when employing low-cost equipment. This translates mathematically to an LPR of the received baseband samples. In fact, CFO creates two sorts of receiver impairments. The first is the CPE, which, may be easily adjusted in the frequency domain. The second is ICI, which is induced by the frequency domain mismatch of the PF of the transmitter and receiver.

Because of its low-frequency localization, the second drawback is a severe problem for OFDM. On the other hand,

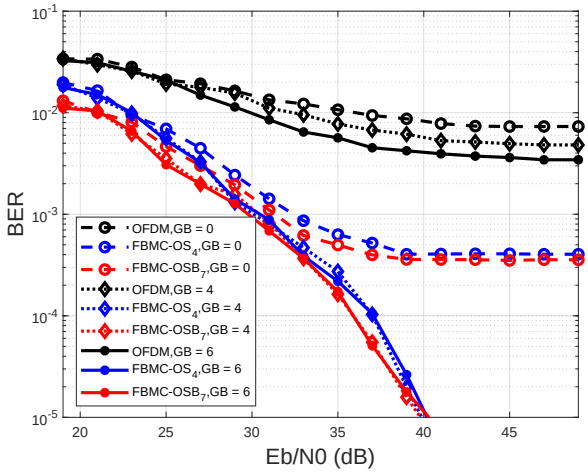

Fig. 6: Comparison of BER performance for all receivers over the 5G Quadriga fading channel under the '3GPP-3D-UMA-NLOS' scenario' considering $P_s = 0$ dBW, with 3 users, and 64 Rx antennas.

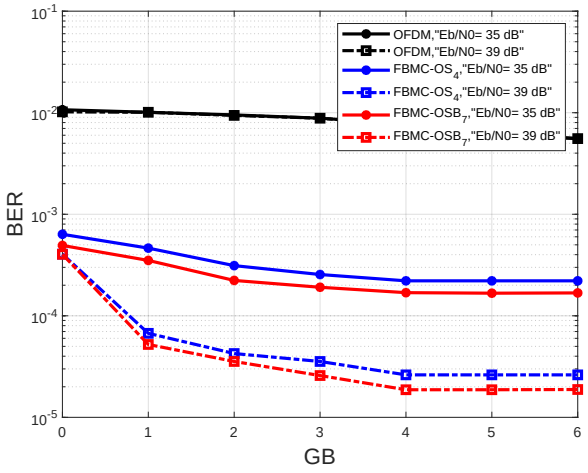

Fig. 7: Comparison of BER performance versus GB size for all receivers over the 5G QuaDRiGa fading channel under the '3GPP-3D-Uma-NLOS' scenario' considering $P_s = 0$ dBW, 3 users, 64 Rx antennas and different E_b/N_0 values.

the frequency domain compensation (FDC) technique, can be used to compensate the CFO for FBMC [17], resulting in a significant reduction in the ICI induced by the CFO. This is a key benefit for FBMC since it relaxes the frequency synchronization requirement, allowing for higher speeds and the use of low-cost oscillators.

In this regard, we study the robustness of each receiver to CFO resulting from the frequency misalignment of local oscillators in terms of SIR. In this case, the CPE term to compensate is $e^{j\pi nr}$ where r is the CFO relative to Δf, which is assumed to be perfectly known at the receiver side.

In order to validate the accuracy of our analytical study for the OS-based receivers in the presence of CFO impairments, we plot in Figure 4 the SIR obtained by simulation for the OS_4-FBMC and the OSB_7-FBMC receivers, as well as the SIR determined by evaluating equations (31) and (33). The results are then compared to the OFDM receiver. As depicted in the figure, the OS receiver is more robust than the OSB-FBMC receiver against CFOs. The simulation results are confirmed analytically as depicted in the same figure. Concerning OFDM, the SIR simulation results also confirm its high sensitivity to CFOs compared to the OS-based FBMC receivers.

VIII. Performance in an asymptotic regime

In this section, we perform the analysis carried out in Section IV-C as well as the efficiency of our proposed receivers in an asymptotic regime. The noise level is chosen so that the signal-to-noise ratio (SNR) at the input of the BS antennas is equal to 10 dB. Note that, the noise contribution fades away as the number of antennas at the BS tends to infinity. The NPR1 PF is used unless explicitly mentioned otherwise. Figure 5 compares the SINR performance for different FBMC receivers over different channels and OFDM is chosen as a benchmark. First, we compared the saturation level for the OS receiver achieved in (69) to that obtained in [25]. For that, the same channel (delay spread = 40 samples) and parameters are used for a fair comparison.

As depicted in the figure, the saturation level obtained for the OS_4-FBMC receiver is 16.2 dB larger than the one obtained in [25]. This confirms the superiority of the OS-FBMC receiver since it was also confirmed analytically using (69) and equation (17) in [25]. It is worth noting that the delay spread (40 samples) of the channel is slightly larger than the CP duration of OFDM (36 samples). Although this represents only a difference of 10%, OFDM fails to outperform the OS_4-FBMC receiver.

It is worth noting that the channel used in [25] is non-realistic and a lower saturation level might be obtained over a realistic one. For that, we compare the SIR saturation level of the OS_4-FBMC receiver to that of a PPN receiver over the 5G channel in the 3D-Uma-NLOS scenario. As depicted in the same figure, the SIR saturation level decreased by around 2.2 dB with the PPN receiver and by 2.1 dB for the OS_4-FBMC receiver. Using a different up-sampling factor for the OS receiver will decrease the SIR saturation level by around 1.1 dB as was confirmed also by simulation.

IX. BER performance in the presence of two interferers

It is well known that the multi-user interference vanishes in mMIMO systems. Therefore, in this section, we consider a communication in which several users transmit data on adjacent frequency bands. However, the communication is done asynchronously in time. As a result, signals arrive with random delays. In this scenario, we examine 3 transmission channels operating in parallel on 1.5 MHz bands (i.e. 4.5 MHz). The transmission located in the middle will be considered as the "main" transmission which will be demodulated by the receiver. The other 2 transmissions will be treated as interferers with the main transmission. The transmit powers of

all transmissions are assumed to be equal and normalized to $P_s = 0$ dBW.

Figure 6 compares the BER performance of all receivers in the context of mMIMO. Several guard band (GB) lengths (in number of subcarriers) are considered. With no guard band (GB = 0), the performance of all receivers is highly degraded due to the high level of interference resulting from adjacent transmissions. Therefore, it is essential to introduce GBs to limit interference at the cost of a reduction in the transmission rate. A compromise between system performance and achieved throughput is hence applied.

When GB = 4, OFDM shows the worst performance due to its low frequency localization. It is highly affected by the adjacent interferers leading to the highest error floor when compared to FBMC. However, FBMC augmented by the OS-based receivers is more robust against adjacent interferers thanks to the frequency localization of the NPR1 PF.

Similar conclusions can be made with GB = 6. Actually, it is worth noting that the BER performance of the OS_4-FBMC and the OSB_7-FBMC receivers is unaffected. This is because there is no interference stemming from adjacent transmissions. In fact, in order to know how many GBs are necessary to avoid any adjacent interference for the OS-based FBMC receivers, we plot in Figure 7 the BER performance of all considered receivers versus the GB size at $E_b/N_0 = 35$ dB and 39 dB.The BER performance of the OS-based FBMC receivers remains constant after 4 GBs, implying that all the adjacent interference is avoided. In contrast, even a GB size of 6 is insufficient to avoid adjacent interference for OFDM.

Similar conclusions can be made with $E_b/N_0 = 39$ dB. Furthermore, despite the increase in the value of E_b/N_0, OFDM does not improve its results compared to the $E_b/N_0 = 35$ dB case. Therefore, we can deduce that FBMC augmented by the OS-based receivers requires less GBs than OFDM. Hence, FBMC is more bandwidth-efficient under such a scenario.

X. Complexity analysis

In this section, we compare the computational complexity of the proposed OS-based FBMC receivers in the context of MU-mMIMO systems with the conventional OFDM receiver in terms of the required number of real-valued multiplications (RMs) for demodulating a single FBMC/OFDM symbol. We represent the required number of RMs for a specific operation x as CRM(x). It is assumed that a single complex multiplier (CM) entails CRM(CM) = 3 RMs.

According to [35], the number of required RMs $\text{CRM}(\text{FFT}_N)$ of a Fourier transform of size N is given by:

$$C_{\text{RM}}\left(\text{FFT}_N\right) = N\log_2(N) - 3N + 4. \tag{72}$$

The analytical expressions detailing the complexity of the examined receivers can be found in Table III. To ensure a fair comparison, the complexity computation accounts for the difference in QAM processing between FBMC (OQAM) and OFDM (classical QAM).

In the case of the OSB receiver, the number of necessary RMs for the FFT of size N is divided by N_s. This accounts for the fact that only one FFT of size N is required to demodulate N_s FBMC symbols within a block.

A notable distinction among the considered receivers lies in the filtering stage. Specifically, the OFDM receiver omits any filtering operation, resulting in CRM(filtering) = 0. In contrast, the OS-based receivers require a filtering operation, and its complexity is contingent on the parameters N_R, U, and Δ.

Therefore, when assuming $M = 512$, $N_c = 300$ $U = 4$, $N_R = 64$, $\Delta = 3$, $N_s = 7$ and $N_U F = 4$, we see that the proposed FBMC-OSB_7 receiver is 55% less complex than the FBMC-OS_4 receiver. Conversely, the OFDM receiver is 58% less complex than the FBMC-OS_4 receiver.

XI. Conclusion

This article extends the use of OS-based FBMC receivers with short filters to the context of MU-mMIMO and investigates their advantages in comparison to OFDM under different channel impairments. The first appealing benefit of the FBMC waveform with OS-based receivers resides in its robustness against timing offsets when compared to OFDM, even enabling asynchronous communications, and relaxed synchronization, as validated in both analytical and simulation studies. Moreover, the robustness of the OS-based FBMC receivers to carrier frequency offsets was confirmed analytically. Furthermore, in the context of mMIMO systems, we performed an asymptotic study on the performance of FBMC augmented with the proposed receivers, and we showed that increasing the number of BS antennas does not allow the SINR to increase unbounded while still outperforming OFDM. In fact, the conducted validation shows that results obtained through the proposed analytical study are in conformity with those obtained through simulations. This provides a significant advantage in terms of predicting system parameters for target impairment/robustness levels, as the time required to obtain results analytically is much shorter. Furthermore, simulation results confirm the superiority of the OS-based FBMC receivers compared to OFDM in the presence of adjacent interferers. Consequently, augmented by the OS-based receivers, the FBMC-OQAM waveform becomes a viable competitor to OFDM in the context of MU-mMIMO.

Acknowledgments

This work was supported in part by the Beyond5G project funded by the French government as part of the economic recovery plan, namely "France Relance", and the investments for the future program and in part by the PEPR 5G and Future Networks project funded by the Agence Nationale de la Recherche (ANR) grant NF-PERSEUS : "ANR-22-PEFT -0004".

Appendix

Table IV presents a list of the main notations used in this paper.

Receiver	FFT	Equalization	Filtering
OFDM	$\mathrm{N}_R\left(\mathrm{C}_{RM}\left(\mathrm{FFT}_M\right)/2\right)$	$3\ \mathrm{N}_R\mathrm{UN}_c/2$	0
FBMC-OS$_{N_{UF}}$	$\mathrm{N}_R\left(\mathrm{C}_{RM}\left(\mathrm{FFT}_M\right)\right)$	$3\ \mathrm{N}_R\mathrm{U}(\mathrm{N}_c+2\Delta)$	$\mathrm{UN}_{UF}\mathrm{N}_c(\Delta+1)$
FBMC-OSB$_{N_s}$	$\mathrm{N}_R\left(\mathrm{C}_{RM}\left(\mathrm{FFT}_M\right)/N_s\right)$	$3\ \mathrm{N}_R\mathrm{U}(\mathrm{N}_c+2\Delta)$	$\mathrm{UN}_{UF}\mathrm{N}_c(\Delta+1)$

TABLE III: Number of real multiplications required for each considered receiver.

Notations	**Description**
l_d	TO value
r	CFO value
n	Time index
$\hat{\boldsymbol{a}}_{\boldsymbol{n}}(m)$	Transmitted PAM symbols
m	Frequency index
$\hat{\boldsymbol{a}}_{\boldsymbol{n}}(m)$	Estimated PAM symbols
$\phi_n(m)$	Phase rotation
h	Channel impulse response
N_R	Number of BS antennas
$\boldsymbol{X}_{\boldsymbol{n}}(m)$	Equalized signal
N_{UF}	Upsampling factor
U	Total number of users
u	User's index
λ	Carrier wavelength
$\rho_{m,u}$	power delay profile (PDP)
H	Channel frequency response
g	Impulse response of the PF
M	Total number of subcarriers
N	FFT size
L	Total number of channel paths
$\boldsymbol{C_{CPE}(n)}$	CPE compensation term
$\boldsymbol{C_{TO}(m)}$	TO compensation term
$\boldsymbol{s}$	Transmitted signal
$\boldsymbol{b}$	Block in a frame
Π	Rectangular function
$\boldsymbol{C}$	Equalizer matrix
N_G	Number of non-truncated filter coefficients

TABLE IV: Table of notations

REFERENCES

[1] Hamdar, F., Nadal, J., Nour, C. A., and Baghdadi, A., "Overlap-Save FBMC receivers for massive MIMO systems under channel impairments," in *IEEE 95th Vehic. Technol. Conf.: (VTC-Spring)*, 2022, pp. 1–7.

[2] Marzetta, T., Larsson, E., Hong, Y., and Ngo, H., *Fundamentals of Massive MIMO*. United Kingdom: Cambridge University Press, 2016.

[3] Ngo, H., *Massive MIMO: Fundamentals and system designs*, Ph.D. dissertation, Linköping Univ., LinkÃűping, Sweden, 2015, department of Electrical Engineering (ISY).

[4] Juwono, F. H. and Reine, R., "Future ofdm-based communication systems towards 6g and beyond: Machine learning approaches," *Green Intelligent Systems and Applications*, vol. 1, no. 1, p. 19–25, Nov. 2021. [Online]. Available: https://tecnoscientifica.com/journal/gisa/article/view/34

[5] Marzetta, T. L., "Noncooperative Cellular Wireless with Unlimited Numbers of Base Station Antennas," *IEEE Trans. on Wirel. Commun.*, vol. 9, no. 11, pp. 3590–3600, 2010.

[6] Nawaz, S. J., Sharma, S. K., Mansoor, B., Patwary, M. N., and Khan, N. M., "Non-coherent and backscatter communications: Enabling ultra-massive connectivity in 6g wireless networks," *IEEE Access*, vol. 9, pp. 38 144–38 186, 2021.

[7] Sathananthan, K. and Tellambura, C., "Probability of error calculation of OFDM systems with frequency offset," *IEEE Trans. on Commun.*, vol. 49, no. 11, pp. 1884–1888, 2001.

[8] Farhang-Boroujeny, B., "OFDM Versus Filter Bank Multicarrier," *IEEE Signal Process. Mag.*, vol. 28, no. 3, pp. 92–112, 2011.

[9] Lim, B. and Ko, Y.-C., "SIR Analysis of OFDM and GFDM Waveforms With Timing Offset, CFO, and Phase Noise," *IEEE Trans. Wirel. Commun.*, vol. 16, no. 10, pp. 6979–6990, 2017.

[10] 3GPP TR 138 901, v15.0.0, "5G; Study on channel model for frequencies from 0.5 to 100 GHz", 2018.

[11] Sabeti, P., Farhang, A., Marchetti, N., and Doyle, L., "CFO Estimation for OFDM-Based Massive MIMO Systems in Asymptotic Regime," in *IEEE 10th Sensor Array and Multichannel Signal Process. Workshop (SAM)*, 2018, pp. 99–103.

[12] Schmidl, T. and Cox, D., "Robust frequency and timing synchronization for OFDM," *IEEE Trans. on Commun.*, vol. 45, no. 12, pp. 1613–1621, 1997.

[13] Vasudevan, K., "Coherent detection of turbo coded ofdm signals transmitted through frequency selective rayleigh fading channels," in *IEEE International Conference on Signal Processing, Computing and Control (ISPCC)*, 2013, pp. 1–6.

[14] ——, "Coherent Detection of Turbo-Coded OFDM Signals Transmitted Through Frequency Selective Rayleigh Fading Channels with Receiver Diversity and Increased Throughput," *Wirel. Personal Commun.*, vol. 82, no. 10, pp. 1623–1653, 2015.

[15] ——, "Near capacity signaling over fading channels using coherent turbo coded ofdm and massive mimo," *International Journal On Advances in Telecommunications issn 1942-2601*, vol. 10, pp. 22–37, 06 2017.

[16] Banelli, P., Buzzi, S., Colavolpe, G., Modenini, A., Rusek, F., and Ugolini, A., "Modulation Formats and Waveforms for 5G Networks: Who Will Be the Heir of OFDM?: An overview of alternative modulation schemes for improved spectral efficiency," *IEEE Signal Proc. Mag.*, vol. 31, no. 6, pp. 80–93, 2014.

[17] Nadal, J., Nour, C. A., and Baghdadi, A., "Design and Evaluation of a Novel Short Prototype Filter for FBMC/OQAM Modulation," *IEEE Access*, vol. 6, pp. 19 610–19 625, 2018.

[18] Nadal, J., Leduc-Primeau, F., Nour, C. A., and Baghdadi, A., "Overlap-save FBMC Receivers," *IEEE Trans. on Wireless Commun.*, vol. 19, no. 8, pp. 5307–5320, 2020.

[19] Bingham, J., "Multicarrier modulation for data transmission: an idea whose time has come," *IEEE Commun. Mag.*, vol. 28, no. 5, pp. 5–14, 1990.

[20] Rusek, F., Persson, D., Lau, B. K., Larsson, E. G., Marzetta, T. L., Edfors, O., and Tufvesson, F., "Scaling Up MIMO: Opportunities and Challenges with Very Large Arrays," *IEEE Signal Process. Mag.*, vol. 30, no. 1, pp. 40–60, 2013.

[21] Hirosaki, B., "An Orthogonally Multiplexed QAM System Using the Discrete Fourier Transform," *IEEE Trans. on Commun.*, vol. 29, no. 7, pp. 982–989, 1981.

[22] Bellanger, M., "FS-FBMC: An alternative scheme for filter bank based multicarrier transmission," in *5th Intl. Symposium on Commun., Control and Signal Process.*, 2012, pp. 1–4.

[23] Farhang, A., Marchetti, N., Doyle, L. E., and Farhang-Boroujeny, B., "Filter Bank Multicarrier for Massive MIMO," in *IEEE 80th Veh. Tech. Conf. (VTC2014-Fall)*, 2014, pp. 1–7.

[24] Hari, K., Baum, D., Rustako, A., Roman, R., and Trinkwon, D., "Channel models for fixed wireless applications," *IEEE 802.16 Broadband Wirel. access working group*, 2003.

[25] Aminjavaheri, A., Farhang, A., Doyle, L. E., and Farhang-Boroujeny, B., "Prototype filter design for FBMC in massive MIMO channels," in *IEEE Intl. Conf. on Commun. (ICC)*, 2017, pp. 1–6.

[26] Tunali, N. E., Wu, M., Dick, C., and Studer, C., "Linear large-scale MIMO data detection for 5G multi-carrier waveform candidates," in *49th Asilomar Conf. on Signals, Systems and Computers*, 2015, pp. 1149–1153.

[27] Materra, D., Tanda, M., and Bellanger, M., "Filter bank multicarrier with PAM modulation for future wirel. systems," in *Signal Proc.*, vol. 120, 2016, p. 594–606.

[28] Jeruchim, M. C., Balaban, P., and Shanmugan, K. S., *Simulation of Communication Systems, Second Edition, New York, Kluwer Academic/Plenum*, 2000.

[29] Osinsky, A., Ivanov, A., and Yarotsky, D., "Theoretical Performance Bound of Uplink Channel Estimation Accuracy in Massive MIMO," in *IEEE Intern. Conf. on Acoustics, Speech and Signal Proc. (ICASSP)*, Barcelona, Spain, 2020, pp. 4925–4929.

[30] Quadriga Channel, "Quasi deterministic radio channel generator user manual and documentation," https://quadriga-channel-model.de/, July 12, 2021.

[31] 3GPP TR 25.996, v14.0.0, "Spatial channel model for multiple input multiple output (MIMO) simulations", 2017.

[32] Kyösti, P., Meinilä, J., Hentilä, L., Zhao, X., Jämsä, Schneider, T., and Christian Milan Narandzić, A. H. J. Y. V.-M. H. M. A. R. B. Y. d. J. T. R., "IST-4-027756 WINNER II D1.1.2 v.1.1: WINNER II channel models," 2007. [Online]. Available: http://www.ist-winner.org

[33] Ivanov, A., Osinsky, A., Lakontsev, D., and Yarotsky, D., "High Performance Interference Suppression in Multi-User Massive MIMO Detector," in *IEEE 91st Veh. Tech. Conf. (VTC2020-Spring)*, 2020.

[34] Liu, G., Hou, X., Jin, W. *et al.*, "3-D-MIMO With Massive Antennas Paves the Way to 5G Enhanced Mobile Broadband: From System Design to Field Trials," *IEEE J. on Selected Areas in Commun.*, vol. 35, no. 6, pp. 1222–1233, 2017.

[35] Sorensen, H., Heideman, M., and Burrus, C., "On computing the split-radix FFT," *IEEE Transactions on Acoustics, Speech, and Signal Processing*, vol. 34, no. 1, pp. 152–156, 1986.